

## A DYNAMICAL MASS CONSTRAINT FOR PRE-MAIN-SEQUENCE EVOLUTIONARY TRACKS: THE BINARY NTT 045251 + 3016

AARON T. STEFFEN AND ROBERT D. MATHIEU

Department of Astronomy, University of Wisconsin, Madison, 475 North Charter Street, Madison, WI 53706-1582; steffen@astro.wisc.edu;  
mathieu@astro.wisc.edu

MARIO G. LATTANZI

Osservatorio Astronomico di Torino, Strada Osservatorio 20, I-10025 Pino Torinese, Italy; lattanzi@gsc2.to.astro.it

DAVID W. LATHAM

Harvard-Smithsonian Center for Astrophysics, 60 Garden Street, Cambridge, MA 02138; dlatham@cfa.harvard.edu

TSEVI MAZEH

School of Physics and Astronomy, Raymond and Beverly Sackler Faculty of Exact Sciences, Tel Aviv University, Tel Aviv 69978, Israel;  
maze@wise.tau.ac.il

L. PRATO<sup>1</sup>

Department of Physics and Astronomy, UCLA, Los Angeles, CA 90095-1562; lprato@astro.ucla.edu

MICHAL SIMON<sup>1</sup>

Department of Physics and Astronomy, State University of New York at Stony Brook, Stony Brook, NY 11794-3800; MSIMON@astro.sunysb.edu

HANS ZINNECKER

Astrophysikalisches Institut Potsdam, An der Sternwarte 16, D-14482 Potsdam, Germany; hzinnecker@aip.de

AND

DAVIDE LOREGGIA

Osservatorio Astronomico di Torino, Strada Osservatorio 20, I-10025 Pino Torinese, Italy; loreggia@to.astro.it

Received 2000 August 29; accepted 2001 May 1

### ABSTRACT

We present an astrometric-spectroscopic orbital solution for the pre-main-sequence binary NTT 045251 + 3016. Interferometric observations with the *HST* Fine Guidance Sensor No. 3 allowed stellar separations as small as 14 mas to be measured. Optical spectra provided 58 radial velocity measurements of the primary star, and near-infrared spectra provided two radial velocity measurements of both the primary and secondary, giving a mass ratio for the binary system. The combination of these data allows the dynamical masses and the distance of the stars to be derived. Our measurements for the primary and secondary masses are  $1.45 \pm 0.19$  and  $0.81 \pm 0.09 M_{\odot}$ , respectively, and  $145 \pm 8$  pc for the distance of the system, consistent with prior estimates for the Taurus-Auriga star-forming region. The evolutionary tracks of D'Antona & Mazzitelli, published in 1997, Baraffe et al., published in 1998, and Palla & Stahler, published in 1999, are tested against these dynamical mass measurements. Because of the intrinsic color- $T_{\text{eff}}$  variation within the K5 spectral class, each pre-main-sequence model provides a mass range for the primary. The theoretical mass range derived from the Baraffe et al. tracks that use a mixing-length parameter of  $\alpha = 1.0$  is closest to our measured primary mass, deviating between 1.3 and 1.6  $\sigma$ . The set of Baraffe et al. tracks that use  $\alpha = 1.9$  deviates between 1.6 and 2.1  $\sigma$  from our measured primary mass. The mass range given by the Palla & Stahler tracks for the primary star deviate between 1.6 and 2.9  $\sigma$ . The D'Antona & Mazzitelli tracks give a mass range that deviates by at least 3.0  $\sigma$  from our derived primary mass, strongly suggesting that these tracks are inconsistent with our observation. Observations of the secondary are less constraining than those of the primary, but the deviations between the dynamical mass of the secondary and the mass inferred for the secondary from the various pre-main-sequence tracks mirror the deviations of the primary star. All the pre-main-sequence tracks are consistent with coequality of the components of NTT 045251 + 3016.

*Key words:* binaries: spectroscopic — binaries: visual — stars: evolution — stars: pre-main-sequence

### 1. INTRODUCTION

Pre-main-sequence (PMS) stellar evolution has been extensively modeled in the last decade. Unfortunately, very few PMS stars have provided detailed observational tests of these models, in large part because of the lack of dynamical

mass determinations. Recently, a precise mass determination has been achieved for the secondary of the eclipsing binary TY CrA (Casey et al. 1998; Corporon, Lagrange, & Beust 1996, and references therein). Casey et al. (1998) tested three sets of evolutionary tracks against the  $1.64 M_{\odot}$  secondary and found that all were consistent with the observed physical parameters. Covino et al. (2000) analyzed the eclipsing binary RXJ 0529.4+0041 and compared the  $1.25 M_{\odot}$  primary star and the  $0.91 M_{\odot}$  secondary star with three sets of evolutionary tracks. They found that the Baraffe et al. (1998) tracks provide the closest agreement with the derived masses of both stars. Stellar masses have also been

<sup>1</sup> Visiting Astronomer, Kitt Peak National Observatory (KPNO), National Optical Astronomy Observatories (NOAO), which are operated by the Association of Universities for Research in Astronomy (AURA), Inc., under cooperative agreement with the National Science Foundation (NSF).

measured via orbital motions of disk gas (see, e.g., Guillo-  
teau, Dutrey, & Simon 1999; Simon, Dutrey, & Guillo-  
teau 2000). This is currently the only technique available for  
obtaining the mass of a single star, but it is limited by  
distance uncertainty. Simon et al. (2000) found that PMS  
evolutionary models that presented cooler  $T_{\text{eff}}$  values (see,  
e.g., Baraffe et al. 1998 and Palla & Stahler 1999) provided a  
better fit with their derived masses of nine PMS stars.  
Another powerful method for stellar mass determination is  
the combination of spectroscopic and astrometric obser-  
vations of a binary star. In addition to all the orbital ele-  
ments, the combination of an angular measure of the orbit  
from astrometry and a linear measure from radial velocities  
allows an independent determination of the binary distance.  
This paper describes such a study of the naked T Tauri  
binary NTT 045251 + 3016.

NTT 045251 + 3016 was first discovered with the *Einstein*  
*Observatory* as an optically visible star associated with an  
X-ray source. Detailed *UBVRIJHKL* photometry and  
optical spectra for the primary star are presented by Walter  
et al. (1988), who derived a K7 spectral classification for  
the primary star and also identified the system as a spectro-  
scopic binary. Improved spectral classification of the  
primary is discussed in § 4.1. Based on a mean radial veloc-  
ity near to that of the Taurus-Auriga association and a Li I  
 $\lambda 6707\text{\AA}$  equivalent width of  $0.58\text{\AA}$ , Walter et al. (1988)  
identified NTT 045251 + 3016 as a PMS star.

NTT 045251 + 3016 is unique among known PMS  
binaries in that it has an orbit with a short enough period to  
permit measurable radial velocity variations of the primary  
and secondary stars while at the same time being wide  
enough to spatially resolve the two stars with *HST*'s Fine  
Guidance Sensor. We describe here an observational  
program to obtain both spectroscopic and astrometric data,  
thereby determining the masses of both PMS stars and the  
distance to the binary.

## 2. OBSERVATIONS

### 2.1. Astrometric

The first interferometric observation of NTT  
045251 + 3016 with the astrometer Fine Guidance Sensor  
No. 3 (FGS3) aboard *HST* was executed on 1995 April 14.

The target was visited on 17 different occasions during the  
subsequent 3.3 yr observing campaign (completed 1998  
August 20), covering approximately one quadrant of the  
apparent orbit. The interferometric mode of FGS3 is used  
to sample the visibility function (VF) produced by the  
Koester's prism interferometer as the field of view of the  
unit is driven across the target. For best results, the FGS  
was commanded to oversample the VF by taking measure-  
ments every 0.6 mas (on the sky) during a scan of  $\sim 1500$   
mas in length. The scan length used is sufficient, during  
normal operations, to encompass the sensitivity range of the  
interferometer, which extends for  $\sim 20$  mas around the line  
of sight to the target. FGS3 is endowed with two Koester's  
prisms that provide sensitivity in two orthogonal directions,  
usually referred to as the FGS *X* and *Y* axes (Lupie &  
Nelán 1998). Therefore, each scan of the target results in  
two VF's that are then independently analyzed for signa-  
tures other than those characteristic of a suitable single (and  
pointlike) star chosen as a template. Deviations from the  
single-star VF provide measures of the projected separa-  
tions of the binary at each observing epoch. The compar-  
ison with the template also provides two independent  
estimates of the magnitude difference between the two com-  
panions. On-sky separation ( $\rho$ ) and astronomical position  
angle (P.A.) are easily derived from the projected separa-  
tions and telescope attitude data (Bernacca et al. 1993).

Fifteen consecutive scans were taken on each visit to  
check on scan-to-scan repeatability and for improvement of  
the signal-to-noise ratio (S/N). The average S/N of the  
observed scans is  $\sim 20$ , which improved to  $\sim 20(15)^{1/2} \sim 80$   
after merging the scans (Lattanzi et al. 1997, and references  
therein). The shape of the visibility curve changes with effec-  
tive wavelength, which can introduce systematic errors if  
the color of the template differs significantly from that of the  
target. To minimize this effect, we selected star SAO 185689  
[ $(B - V) = 1.5\text{ mag}$ ] as the template single star. Among the  
templates made available by the STScI for FGS reductions,  
this is the star with the color closest to that of our binary  
[observed  $(B - V) = 1.28\text{ mag}$ ].

Fourteen of the 17 visits produced successful measure-  
ments of the binary separation and orientation. These mea-  
surements are listed in Table 1. The 85% success rate is  
gratifying given both the small separation ( $\sim 3$  times

TABLE 1  
RELATIVE ASTROMETRIC MEASUREMENTS OF NTT 045251 + 3016

HJD	$\Delta m_x$ (mag)	$\Delta m_y$ (mag)	P.A. <sup>a</sup> (deg)	$\rho$ (arcsec)	P.A. ( <i>O</i> - <i>C</i> ) (deg)	$\rho$ ( <i>O</i> - <i>C</i> ) (arcsec)	Phase
2,449,822.0.....	2.0	2.2	187	0.046	7.20	0.0052	2.277
2,450,038.0.....	2.1	2.6	178	0.048	4.75	0.0041	2.363
2,450,098.0.....	2.4	2.2	170	0.048	-1.53	0.0041	2.386
2,450,161.0.....	1.9	2.2	169	0.042	-0.68	-0.0016	2.412
2,450,317.0.....	2.7	2.5	163	0.041	-1.99	-0.0005	2.473
2,450,372.0.....	2.2	2.5	160	0.036	-3.17	-0.0043	2.495
2,450,480.0.....	2.4	2.4	158	0.039	-1.27	0.0015	2.537
2,450,538.0.....	2.3	2.6	153	0.037	-3.88	0.0013	2.560
2,450,669.0.....	2.1	2.2	149	0.031	-1.36	0.0000	2.612
2,450,705.0.....	1.7	2.7	146	0.029	-2.19	-0.0005	2.626
2,450,767.0.....	2.1	2.2	138	0.016	-5.89	-0.0110	2.651
2,450,882.0.....	2.6	1.8	124	0.014	-9.21	-0.0081	2.697
2,450,913.0.....	2.2	2.4	121	0.023	-8.48	0.0022	2.709
2,451,046.0.....	2.5	2.1	120	0.018	12.93	0.0020	2.762

<sup>a</sup> The P.A. is measured north through east.

smaller than the Airy angular resolution limit at visible light) and the relatively large magnitude difference (more than 2 mag).

The formal error of the projected separations is  $\sim 1$  mas on each axis. However, this error is internal, since it only takes into account the contribution from the reduction method, which is based on an analytical cross-correlation technique (Bernacca et al. 1993). There are other error sources that are known to be present but are difficult to quantify for each observation. As an example, the epochs of observation of the calibration star are usually quite different (up to 5 months) from the dates of the visits to our target; consequently, the template star might not be the best representation of the FGS signatures at the time of the science observation, since small changes are known to occur even on relatively short timescales. By comparing observations of the template star taken at different times, we have measured variations in the structure of the VF, which could increase the separation measurement error to 2–3 mas. Therefore, this is probably a more realistic range for the error of several of the measured projected separations in Table 1. This corresponds to 3–4 mas for the ( $1\sigma$ ) error in total separation and to  $\sim 14^\circ$  for the maximum error in P.A.

Table 1 also shows the measurements of the visual magnitude difference between the two companions. The values derived from the independent fits to the  $X$  and  $Y$  VF's are generally in good agreement, except for the 10th and 12th measurements. Averaging the results yields  $\Delta m_X \simeq 2.2 \pm 0.3$  mag and  $\Delta m_Y \simeq 2.3 \pm 0.3$  mag for the average magnitude differences on the  $X$  and  $Y$  axes, respectively. Again, these results are consistent with instrument performances expected in a challenging scenario like ours, i.e., small separation and relatively large magnitude difference.

## 2.2. Optical Radial Velocities

Since 1985, we have monitored the radial velocity of NTT 045251 + 3016 with the Center for Astrophysics (CfA) Digital Speedometers (Latham 1992). Three nearly identical instruments were used on the Multiple Mirror Telescope, the 1.5 m Tillinghast Reflector at the Whipple Observatory atop Mount Hopkins, Arizona, and the 1.5 m Wyeth Reflector located in Harvard, Massachusetts. Echelle spectrographs were used with intensified photon-counting Reticon detectors to record about  $45 \text{ \AA}$  of spectrum in a single order centered near  $5187 \text{ \AA}$ , with a resolution of about  $8.3 \text{ km s}^{-1}$  and S/Ns ranging from 8 to 15 per resolution element.

Radial velocities were derived from the 58 observed optical spectra using the one-dimensional correlation package RVSAO (Kurtz & Mink 1998) running inside the IRAF<sup>2</sup> environment. The template spectrum was drawn from a new grid of synthetic spectra (Morse & Kurucz 2001) calculated using model atmospheres computed using Kurucz's code, ATLAS9. We correlated our observed spectra against a grid of solar metallicity templates and chose the one that gave the highest average peak correlation.

The highest peak correlation averaged over all 58 observed spectra was obtained for  $T_{\text{eff}} = 4500 \text{ K}$ ,  $\log g = 3.5 \text{ cm s}^{-2}$ ,  $[M/H] = 0.0$ , and  $v \sin i = 10 \text{ km s}^{-1}$ . The heliocentric velocities derived with this template are reported in Table 2, together with the heliocentric Julian

TABLE 2  
OPTICAL RADIAL VELOCITY MEASUREMENTS FOR  
NTT 045251 + 3016

HJD	$v_1$ ( $\text{km s}^{-1}$ )	$v_1 (O-C)$ ( $\text{km s}^{-1}$ )	Phase
2,446,421.7465.....	4.52	-0.47	0.930
2,446,428.6909.....	5.26	0.39	0.933
2,446,451.6493.....	3.38	-1.12	0.942
2,446,728.8724.....	11.84	0.45	1.052
2,446,775.7779.....	13.31	0.04	1.071
2,446,804.6601.....	13.92	-0.34	1.082
2,447,045.0073.....	18.00	-0.35	1.177
2,447,075.8236.....	18.86	0.30	1.189
2,447,080.8803.....	17.56	-1.03	1.191
2,447,127.8694.....	19.15	0.34	1.210
2,447,138.7852.....	18.99	0.14	1.214
2,447,157.5923.....	19.36	0.44	1.222
2,447,192.6571.....	18.86	-0.15	1.236
2,447,198.6334.....	20.13	1.11	1.238
2,447,427.9813.....	19.53	0.51	1.329
2,447,492.8084.....	19.37	0.47	1.355
2,447,546.5820.....	19.49	0.71	1.376
2,447,576.6672.....	18.96	0.26	1.388
2,447,791.0071.....	16.73	-1.21	1.473
2,447,818.8032.....	18.62	0.80	1.484
2,447,837.7737.....	16.72	-1.01	1.491
2,447,868.9265.....	17.52	-0.07	1.504
2,447,899.5659.....	17.73	0.29	1.516
2,447,928.6599.....	15.84	-1.45	1.527
2,447,957.6175.....	17.40	0.26	1.539
2,447,965.6088.....	17.31	0.22	1.542
2,448,168.9077.....	15.89	0.06	1.622
2,448,194.9668.....	15.10	-0.54	1.633
2,448,284.7375.....	14.39	-0.55	1.668
2,448,635.7208.....	11.43	0.46	1.807
2,448,669.5847.....	11.13	0.70	1.821
2,448,675.6738.....	11.39	1.06	1.823
2,448,697.6311.....	10.25	0.28	1.832
2,448,875.9712.....	6.05	-0.38	1.902
2,448,901.9111.....	5.34	-0.54	1.913
2,448,910.8049.....	6.41	0.72	1.916
2,448,931.9191.....	6.84	1.57	1.925
2,448,970.8280.....	4.23	-0.36	1.940
2,448,988.7716.....	5.38	1.04	1.947
2,449,030.7093.....	3.75	-0.31	1.964
2,449,056.6040.....	3.41	-0.74	1.974
2,449,235.0189.....	11.21	0.67	2.045
2,449,258.9979.....	12.14	0.52	2.054
2,449,290.8841.....	13.23	0.32	2.067
2,449,316.8181.....	13.11	-0.73	2.077
2,449,318.8322.....	13.72	-0.19	2.078
2,449,379.6724.....	14.56	-1.09	2.102
2,449,652.0326.....	18.03	-0.78	2.210
2,449,706.8549.....	17.98	-1.00	2.231
2,450,000.9524.....	19.19	0.25	2.348
2,450,029.9190.....	18.76	-0.12	2.359
2,450,087.7501.....	18.47	-0.26	2.382
2,450,173.5382.....	19.51	1.04	2.416
2,450,771.7774.....	16.51	1.26	2.653
2,450,771.7982.....	14.68	-0.57	2.653
2,450,799.9570.....	14.96	-0.06	2.664
2,451,563.5879.....	2.21	-1.85	2.967
2,451,570.4936.....	5.53	1.45	2.970

date and  $O-C$  errors. The rms deviation about the orbital solution is  $0.7 \text{ km s}^{-1}$ , typical of CfA precision for late-type dwarfs. An implicit assumption of our analysis is that the spectra of PMS stars can be reliably modeled using normal

<sup>2</sup> IRAF is distributed by the NOAO, which are operated by AURA, Inc., under cooperative agreement with the NSF.

TABLE 3  
IR RADIAL VELOCITY MEASUREMENTS FOR NTT 045251 + 3016

HJD	$v_1$ (km s <sup>-1</sup> )	$v_1 (O-C)$ (km s <sup>-1</sup> )	$v_2$ (km s <sup>-1</sup> )	$v_2 (O-C)$ (km s <sup>-1</sup> )	Phase
2,451,529.7500.....	4.1	-0.08	33.6	0.70	2.953
2,451,530.7500.....	3.4	-0.77	31.6	-1.04	2.954

stellar atmospheres. However, a small template mismatch would not significantly affect the accuracy of the radial velocity measurements.

We attempted to detect the secondary spectrum in the optical with high S/N observations of NTT 045251 + 3016 taken in 1992 February, near a time of maximum velocity separation, with the Hamilton echelle spectrograph on the 3 m Shane Telescope of Lick Observatory. The wavelength region covered was from 3800 to 9800 Å with a S/N of 30. Cross-correlating our high S/N spectrum with a variety of templates did not reveal the secondary's spectrum. To test our detection limits, C. Dolan created synthetic double-lined spectra using a narrow-lined K6 V spectral standard rotationally broadened to 10 km s<sup>-1</sup> to match the rotationally broadened spectrum of NTT 045251 + 3016. This primary spectrum was combined with numerous secondary spectra ranging in spectral type K2 V to M2 V, in rotational velocities (5–50 km s<sup>-1</sup>), in mass ratios (1.0–0.5), and in flux ratios (1.0–0.05). Dolan found that to detect the secondary's spectrum a minimum flux ratio of ~0.2–0.4 is required, except in cases with extreme rotational broadening (greater than 40 km s<sup>-1</sup>) when the secondary becomes undetectable even with a luminosity ratio of 1.0. Thus, our nondetection is consistent with our FGS-determined magnitude difference of 2.4 mag in *V*, corresponding to a flux ratio of 0.11.

### 2.3. Near-Infrared Radial Velocities

Since we were unable to detect the secondary in the optical, we obtained two spectra of the binary with PHOENIX, the KPNO high-resolution near-infrared spectrograph on the 4 m Mayall Telescope. Details on this work are given in Mazeh et al. (2000, 2001).

The central wavelength of the observations was 1.555 μm and yielded a free spectral range of ~1450 km s<sup>-1</sup>; the effective resolution was 35,000. We also observed a sample of 12 main-sequence spectral type standards from F6 through M7 in order to provide templates for a two-dimensional cross-correlation analysis using TODCOR (Zucker & Mazeh 1994). We successfully detected the secondary spectrum using the spectra of HR 8085 (61 Cyg A; K5) and HR 8086 (61 Cyg B; K7), each rotationally broadened by 15 km s<sup>-1</sup>, as the primary and secondary templates, respectively. The velocities are given in Table 3. Our derived flux ratio at 1.555 μm is 0.4 ± 0.1.

To estimate our uncertainty because of template mismatch, we used TODCOR to derive the velocity of each template with regard to the other templates. The scatter of these derived velocities is less than 0.7 km s<sup>-1</sup>. This error is added in quadrature to the estimated uncertainty of the peak location of each spectrum for a total uncertainty of 0.9 km s<sup>-1</sup>. The radial velocities of the primary derived from these near-infrared spectra are consistent to within this uncertainty with the radial velocities predicted by the primary orbital solution at the same epoch, which suggests

that our radial velocity zero point is also accurate at this level.

### 3. ORBITAL SOLUTION

Nine of the relative orbital elements of NTT 045251 + 3016 were calculated via a simultaneous fit to the relative astrometric and primary radial velocity data using a program generously provided by G. Torres. Table 4 shows the orbital elements of the binary NTT 045251 + 3016. The astrometric and spectroscopic data and orbital solutions are presented in Figures 1 and 2, respectively. Although the orbital solution is solved via a simultaneous fit to both the relative astrometric and primary radial velocity data, the large number of radial velocity measurements provide a strong constraint on the elements of the orbital solution that can be calculated with single-lined spectroscopic data (i.e.,  $P$ ,  $\gamma$ ,  $K_1$ ,  $e$ ,  $\omega$ , and  $T$ ). Thus, in practice, the orbital parameters that are being determined with the astrometric data are the angular size of the semimajor axis ( $a$  [in arcsec]), the position angle of the line of nodes ( $\Omega_{2000}$ ), and the inclination angle ( $i$ ).

Furthermore, the only parameter influencing the mass determination, which is derived from the astrometric data, is the inclination. As can be seen from the orientation of the line of nodes in Figure 1, the inclination is quite well constrained by the phase coverage of these data. The distance to the system, essentially set by the angular semimajor axis, is more sensitive to the partial phase coverage and possible systematic errors in the FGS astrometry.

With detection of the secondary in the near-infrared spectra, the mass ratio,  $q$ , was calculated using the *calcu-*

TABLE 4  
ORBITAL ELEMENTS FOR NTT 045251 + 3016  
(ASTROMETRIC-SPECTROSCOPIC SOLUTION)

Parameters	Values
Period (yr) .....	6.913 ± 0.033
$a$ (arcsec) .....	0.0328 ± 0.0013
$e$ .....	0.457 ± 0.017
$i$ (deg) .....	113.8 ± 3.4
$\omega$ (deg) .....	216.7 ± 2.8
$\Omega_{2000}$ (deg) .....	179.5 ± 2.7
$T_0$ .....	1993.369 ± 0.042
$K_1$ (km s <sup>-1</sup> ) .....	7.53 ± 0.16
$K_2$ (km s <sup>-1</sup> ) .....	13.52 ± 0.67
$\gamma$ (km s <sup>-1</sup> ) .....	14.35 ± 0.11
$a$ (AU) .....	4.75 ± 0.33
distance (pc) .....	144.8 ± 8.3
$M_1$ ( $M_\odot$ ) .....	1.45 ± 0.19
$M_2$ ( $M_\odot$ ) .....	0.81 ± 0.09
$M_1 + M_2$ ( $M_\odot$ ) .....	2.26 ± 0.21
$q \equiv M_2/M_1$ .....	0.56 ± 0.03

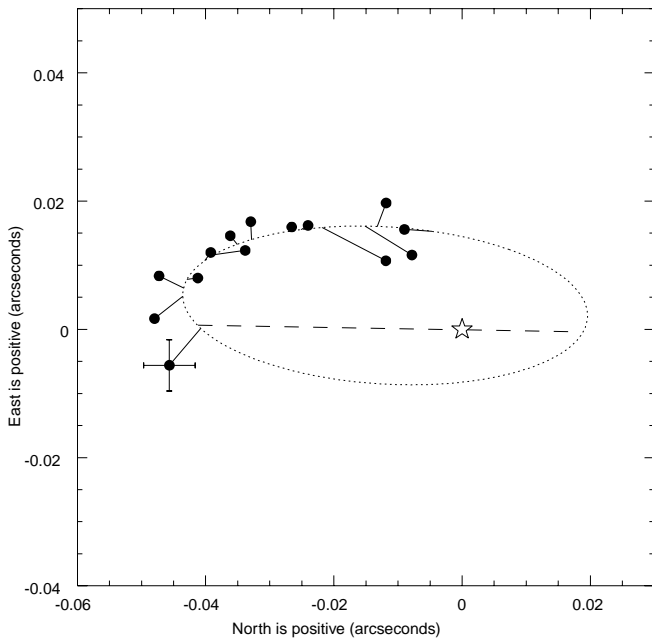


FIG. 1.—Relative astrometric orbit. The filled circles are *HST* FGS measurements, with lines indicating the predicted positions from orbital solution. Here 4 mas error bars are shown on the first observation. The star symbol shows the position of the primary star. The dashed line represents the line of nodes.

lated radial velocity of the primary from the orbital solution at the time of the near-infrared observations, the center-of-mass velocity of the binary, and the mean of the two measured radial velocities of the secondary, which were obtained from IR spectra. This mass ratio, in combination with the nine known orbital elements, allowed us to calcu-

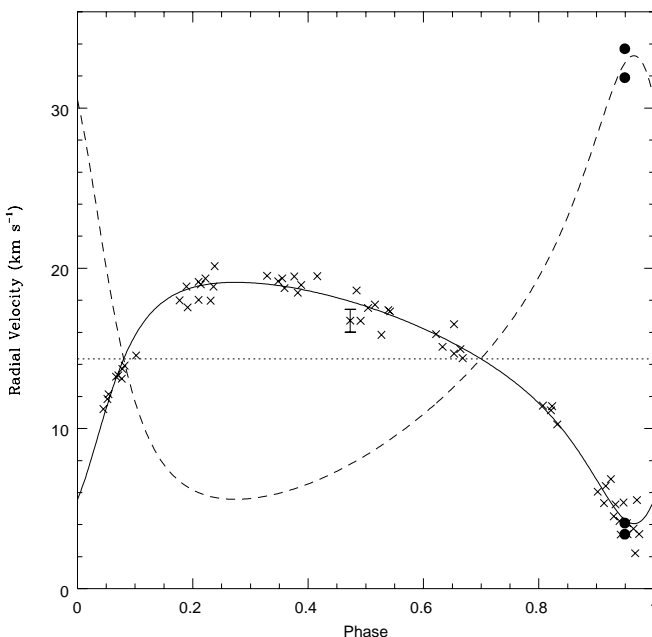


FIG. 2.—Primary (solid line) and secondary (dashed line) spectroscopic orbit solutions and observed radial velocities. Optical data are presented as crosses, and near-infrared data are presented as filled circles. The dotted line is the center-of-mass ( $\gamma$ ) velocity of the orbital solution. Here  $0.7 \text{ km s}^{-1}$  error bars appear on a central point.

late the individual masses of the stars in the binary and the distance to the system.

The masses of the primary and secondary stars are given by the equations (Batten 1973)

$$M_1 (M_\odot) = \frac{3.793 \times 10^{-53} \sqrt{(1-e^2)} (K_1 + K_1/q)^2 (K_1/q) P}{(\sin i)^3}, \quad (1)$$

$$M_2 (M_\odot) = \frac{3.793 \times 10^{-53} \sqrt{(1-e^2)} (K_1 + K_1/q)^2 K_1 P}{(\sin i)^3}, \quad (2)$$

where  $P$  is in years and  $K_1$  is in kilometers per second.

We determine the masses of the primary and secondary to be  $1.45 \pm 0.19$  and  $0.81 \pm 0.09 M_\odot$ , respectively. From equation (1), we find that the largest contributors to the variance of the dynamical mass of the primary are the measurement error associated with the radial velocity of the secondary (39% of the variance) and the error in the measurement of the orbital inclination (38%). The largest contributor to the variance of the secondary's dynamical mass comes from the error associated with the orbital inclination of the binary (54%), followed by the error associated with the measured radial velocity of the secondary (17%). We note that the mass uncertainties associated with our limited number of secondary radial velocity measurements can be reduced substantially with additional observations; higher precision astrometry awaits future instrumentation.

The dynamical distance  $d$ , in parsecs, is given by

$$d = \frac{0.03357 \sqrt{(1-e^2)} (K_1 + K_1/q) P}{a \sin i}, \quad (3)$$

where  $a$  is in arcseconds. Our direct distance measurement to the PMS binary of  $145 \pm 8 \text{ pc}$  agrees with prior distance estimates to the Taurus-Auriga complex based on indirect methods (e.g.,  $140 \pm 10 \text{ pc}$ ; Kenyon, Dobrzycka, & Hartmann 1994) and geometric parallax (e.g.,  $139^{+10}_-9 \text{ pc}$ , Bertout, Robichon, & Arenou 1999; and  $142 \pm 14 \text{ pc}$ , Wichmann et al. 1998). The center-of-mass velocity of the system,  $14.35 \pm 0.11$ , is somewhat lower than the mean radial velocity of the Taurus-Auriga complex ( $17.4 \text{ km s}^{-1}$ ; Hartmann et al. 1986). However, with an association velocity dispersion of  $2 \text{ km s}^{-1}$ , the binary radial velocity is consistent with membership in the association. In this context, we also note that the binary is located at the edge of the association in the Auriga subcomplex.

The largest contributor to the variance of the distance to NTT 045251 + 3016 comes from the error in the measurement of the angular semimajor axis (50%). Since our astrometric data cover only a little more than one quadrant of the orbit, it does not provide a tight constraint on the measurement of the angular semimajor axis (see Fig. 1). Table 4 summarizes our measured masses of, as well as distance to, the components of NTT 045251 + 3016.

#### 4. COMPARISON WITH PMS EVOLUTIONARY MODELS

There are now a variety of PMS models that provide the luminosity and effective temperature of a star given its mass and age. The differences between these models lie largely in

the choice of opacities, atmospheres, metallicities, and convection models. In principle, a PMS star of known mass, luminosity, effective temperature, and metallicity can distinguish between these differences in stellar physics. NTT 045251 + 3016 provides such a case.

#### 4.1. Primary Star

The primary star of NTT 045251 + 3016 was originally classified as a K7 spectral type (Walter et al. 1988). However, analysis of eight temperature-sensitive lines used for spectral classification by Lee (1992;  $\text{V I } 6040 \text{ \AA}$ ,  $\text{Fe I } 6042 \text{ \AA}$ ,  $\text{Fe I } 6056 \text{ \AA}$ ,  $\text{V I } 6058 \text{ \AA}$ ,  $\text{Ni I } 6108 \text{ \AA}$ ,  $\text{V I } 6112 \text{ \AA}$ ,  $\text{Fe I } 6200 \text{ \AA}$ , and  $\text{Sc I } 6211 \text{ \AA}$ ) in our Hamilton echelle spectra clearly point to a K5 classification with an uncertainty of less than one subtype. The Fe I and Sc I line pair around 6200  $\text{\AA}$ , in particular, was used by Basri & Batalha (1990) for spectral classification. Figure 3 compares this line pair from our spectra with three spectral standards, HR 8832 (K3 V), HR 8085 (K5 V), and HR 8086 (K7 V).

Using the photometry of Walter et al. (1988), the luminosity ratios in  $V$  and  $H$ , and the intrinsic colors, temperature calibrations, and bolometric corrections from Kenyon & Hartmann (1995), we find for the primary star an effective temperature of 4350 K and a luminosity of  $0.75 L_{\odot}$ . Since we do not have a luminosity ratio in  $B$  and thus could not calculate the  $B$  magnitude for the primary and secondary individually, we calculated the extinction in  $V$  using two different methods. First we assumed that the secondary did not contribute to the light in the  $B$  band, so the  $B$  magnitude calculated in Walter et al. (1988;  $B = 12.88$ ) was the  $B$  magnitude of the primary. Using this observed  $B$  magnitude and the calculated  $V$  magnitude of the primary with the  $B - V$  color for a K5 dwarf, provided by Kenyon & Hartmann (1995), we obtained an  $E(B - V) = 0.0$ , so this method implied no extinction to the star NTT 045251 + 3016. Alternatively, we assumed the  $H$  band was unaffected by extinction and compared the calculated  $V - H$  for the primary with the  $V - H$  for a K5 dwarf given in Kenyon & Hartmann (1995), finding a visual extinction of  $A_V = 0.15 \pm 0.09$  mag for the primary of NTT 045251 + 3016. We adopt  $A_V = 0.15$  mag throughout this paper.

Since there are temperature and color variations within the K5 spectral class, we define the range of these parameters by the midpoints between the values given for a K5 type and the values for K3 and K7 types, respectively. These upper and lower limits on temperature or color are shown in Figures 4, 5, and 6 as separate points connected by a solid line. This line represents the maximum error range in temperature or color based on our spectral type uncertainty, not a random error. The smaller distance uncertainties and photometric uncertainties are represented as error bars on each point. Table 5 tabulates these stellar parameters and uncertainties for the primary and secondary (§ 4.2) of NTT 045251 + 3016.

Two sets of Baraffe et al. (1998, BCAH98) tracks are plotted on  $M_V - (V - H)$  color-magnitude diagrams (CMDs) with NTT 045251 + 3016 (Fig. 4). Since the solar metallicity template provided the strongest correlation when analyzing the optical spectra, we only test tracks with solar metallicity. BCAH98’s use of the nongray “NextGen” atmosphere models of Hauschildt, Allard, & Baron (1999) allows their tracks to be plotted directly on CMD diagrams. The use of nongray atmosphere models is superior because gray atmospheres tend to overestimate the luminosity and effective temperature of a star of a given mass (BCAH98, and references therein). In addition, BCAH98 argue that CMDs are superior to luminosity- $T_{\text{eff}}$  diagrams because the latter usually depend upon empirically based color- $T_{\text{eff}}$  or color-bolometric corrections, which are derived from a stellar sample with a range of metallicities, gravities, and ages.

The PMS model that provides the closest agreement with our dynamical primary mass is given by the BCAH98 tracks that use a general mixing-length parameter  $\alpha = l/H_p = 1.0$ ,  $[M/H] = 0.0$ , and  $Y = 0.275$ . These tracks predict the mass of the primary to be between 1.15–1.20  $M_{\odot}$ . As seen in Figure 4, this mass range deviates between 1.3 and 1.6  $\sigma$  from our dynamical primary mass measurement.

The second set of PMS tracks shown in Figure 4 were designed by BCAH98 to reproduce the properties of the Sun at 4.61 Gyr. The primary modification in these tracks is an increase in the mixing-length parameter,  $\alpha$ , along with a small change in the Helium abundance ( $\alpha = 1.9$  and  $Y = 0.28$ ). Using these tracks, the derived mass range of the primary is 1.05–1.15  $M_{\odot}$ , which is 1.6–2.1  $\sigma$  from our dynamical primary mass. Thus, while models with this increased mixing-length parameter do not provide as close agreement with our measured dynamical mass as  $\alpha = 1.0$  models, they are nonetheless consistent with our measurements. While the difference between these two mixing-length parameters is rather inconsequential below  $\sim 0.6 M_{\odot}$ , it becomes important for stars above this mass (BCAH98).

Recently, Palla & Stahler (1999, hereafter PS99) calculated a set of PMS tracks to model the star formation history of the Orion Nebula Cluster. These tracks use the initial properties of the protostellar environment to create a well-defined birthline in the H-R diagram (PS99, and references therein). This birthline assists in providing more accurate age estimates to stars that have formed from the same environment.

The PS99 tracks use a gray atmosphere approximation and employ the opacities of Alexander & Ferguson (1994) for low temperatures and the OPAL opacities of Iglesias & Rogers (1996) for high temperatures (greater than  $10^4$  K) with a composition  $X = 0.70$ ,  $Y = 0.28$  (PS99). Convection is treated using mixing-length theory (MLT) with  $\alpha = 1.5$ . Figure 5 displays the PS99 tracks with NTT 045251 + 3016.

TABLE 5  
PARAMETERS AND UNCERTAINTIES FOR NTT 045251 + 3016

Type	Location	$\log(T_{\text{eff}})$	$\log(L_*/L_{\odot})$	$(V - H)_0$	$M_V$
Primary .....	Central point	3.638	$-0.122 \pm 0.053$	$2.74 \pm 0.09$	$5.77 \pm 0.13$
	Lower limit	3.624	$-0.138 \pm 0.053$	$2.88 \pm 0.09$	$5.91 \pm 0.13$
	Upper limit	3.657	$-0.106 \pm 0.053$	$2.53 \pm 0.09$	$5.56 \pm 0.13$
Secondary .....	...	$3.550^{+0.017}_{-0.009}$	$-0.514 \pm 0.086$	$4.04 \pm 0.33$	$8.06 \pm 0.22$

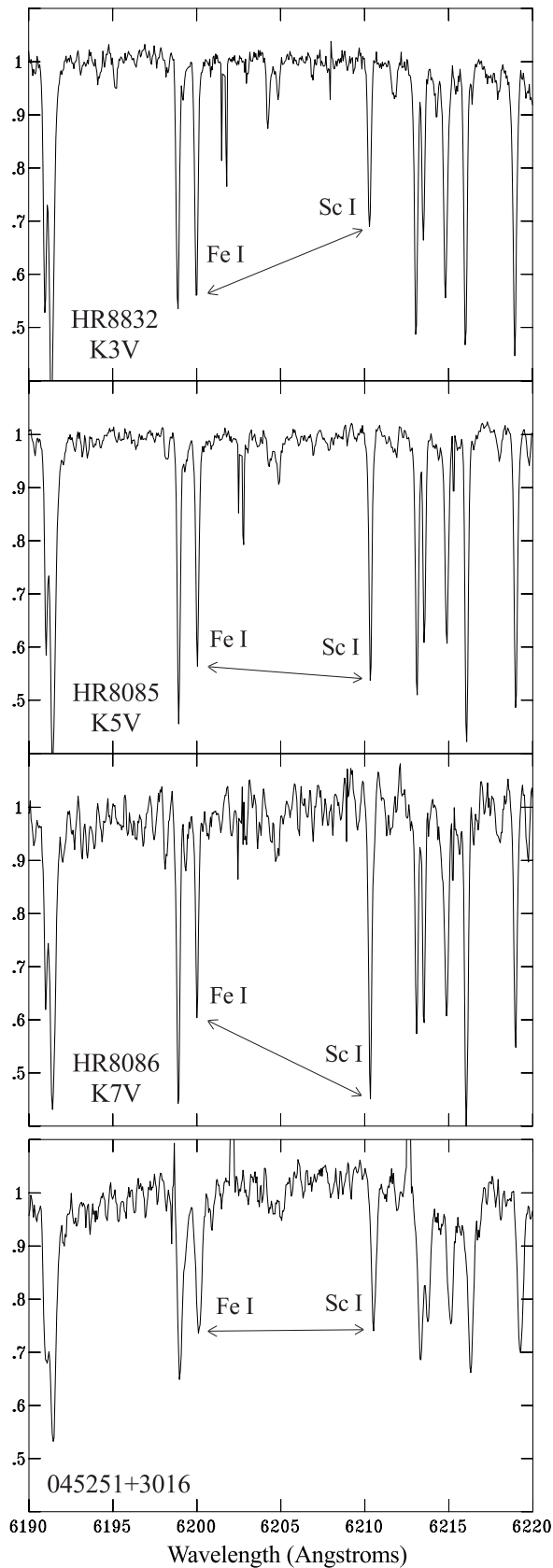


FIG. 3.—Fe I 6200 Å and Sc I 6211 Å line pair used for spectral classification. Spectra are shown for K3, K5, and K7 spectral type standards, along with NTT 045251 + 3016. A three-point smoothing was performed on the spectrum of NTT 045251 + 3016 for presentation purposes.

The mass range of  $0.90\text{--}1.15 M_{\odot}$  given to NTT 045251 + 3016 by the PS99 tracks deviates from our measured primary mass by  $1.6\text{--}2.9 \sigma$ .

Our final comparison is with the PMS tracks of D’Antona & Mazzitelli (1997, hereafter DM97). In 1994, D’Antona & Mazzitelli released a set of PMS tracks that did not use standard MLT to model the convection within the stellar envelope, but instead treated the extended envelope of a PMS star with a “multiple eddy” model called the Full Spectrum of Turbulence (FST) model (Canuto & Mazzitelli 1991). In 1997, D’Antona & Mazzitelli released a new set of PMS tracks that used the updated FST convection model from Canuto, Goldman, & Mazzitelli (1996).

Figure 6 shows the DM97 tracks that provide the closest agreement with our dynamical mass of NTT 045251 + 3016. This set of tracks uses  $Z = 0.02$ ,  $Y = 0.28$  and a deuterium mass fraction of  $1 \times 10^{-5}$ . Nonetheless, the mass range given by DM97 for NTT 045251 + 3016 ( $0.60\text{--}0.87 M_{\odot}$ ) deviates between  $3.0$  and  $4.5 \sigma$  from our dynamical primary mass measurement. From this result, we conclude that the theoretical tracks provided by DM97 are not in agreement with our observational results.

#### 4.2. Secondary Star

Given the flux ratio for the binary in two colors,  $V$  and  $H$ , it is possible to use the photometry presented in Walter et al. (1988) and the intrinsic colors of Kenyon & Hartman (1995) to deduce the spectral type of the secondary. Using the extinction coefficient calculated earlier ( $A_V = 0.15$  mag), we calculate  $(V - H)_0 = 2.74 \pm 0.09$  for the primary star. Applying the observed flux ratios of  $0.12 \pm 0.03$  and  $0.4 \pm 0.1$  in the  $V$  and  $H$  bands, respectively, we determine that for the secondary  $(V - H)_0 = 4.04 \pm 0.33$ . The uncertainty associated with the flux ratio in the  $V$  and  $H$  bands is the main source of the uncertainty in the observed color of the secondary. This color corresponds to an M2 spectral type plus or minus one subclass. The  $T_{\text{eff}}$  was calculated from the  $V - H$  color for the secondary by interpolating in Kenyon & Hartmann (1995). The stellar parameters of the secondary are tabulated in Table 5.

Knowledge of the mass ( $0.81 \pm 0.09 M_{\odot}$ ),  $T_{\text{eff}}$ , and luminosity of the secondary not only provides another constraint for the mass calibration of the PMS models, but it also provides a test of the isochrones for each PMS model, if we assume coevality of the primary and secondary. The issue of coevality in binary formation is not yet well understood (see, e.g., Hartigan, Strom, & Strom 1994), but the relatively old age ( $\sim 3\text{--}10$  Myr) of the NTT 045251 + 3016 pair makes zero-point issues in age comparisons less of a concern. In addition, we argue that the small physical separation of the stars in the binary ( $4.75 \pm 0.33$  AU) suggests that both stars formed together rather than through capture or exchange.

The BCAH98 PMS model, which provides the best agreement with our dynamical primary mass ( $\alpha = 1.0$ ), also provides the best agreement with our dynamical secondary mass. The secondary mass of  $0.73 M_{\odot}$  predicted by the models is within  $1.0 \sigma$  of our dynamical mass measurement. The isochrones are consistent with coevality of the two stars in the binary and predict the age of the components of the binary to be approximately  $1.3 \times 10^7$  yr.

The BCAH98 PMS model that uses a mixing-length parameter  $\alpha = 1.9$  predicts a mass of  $0.67 M_{\odot}$  for the sec-

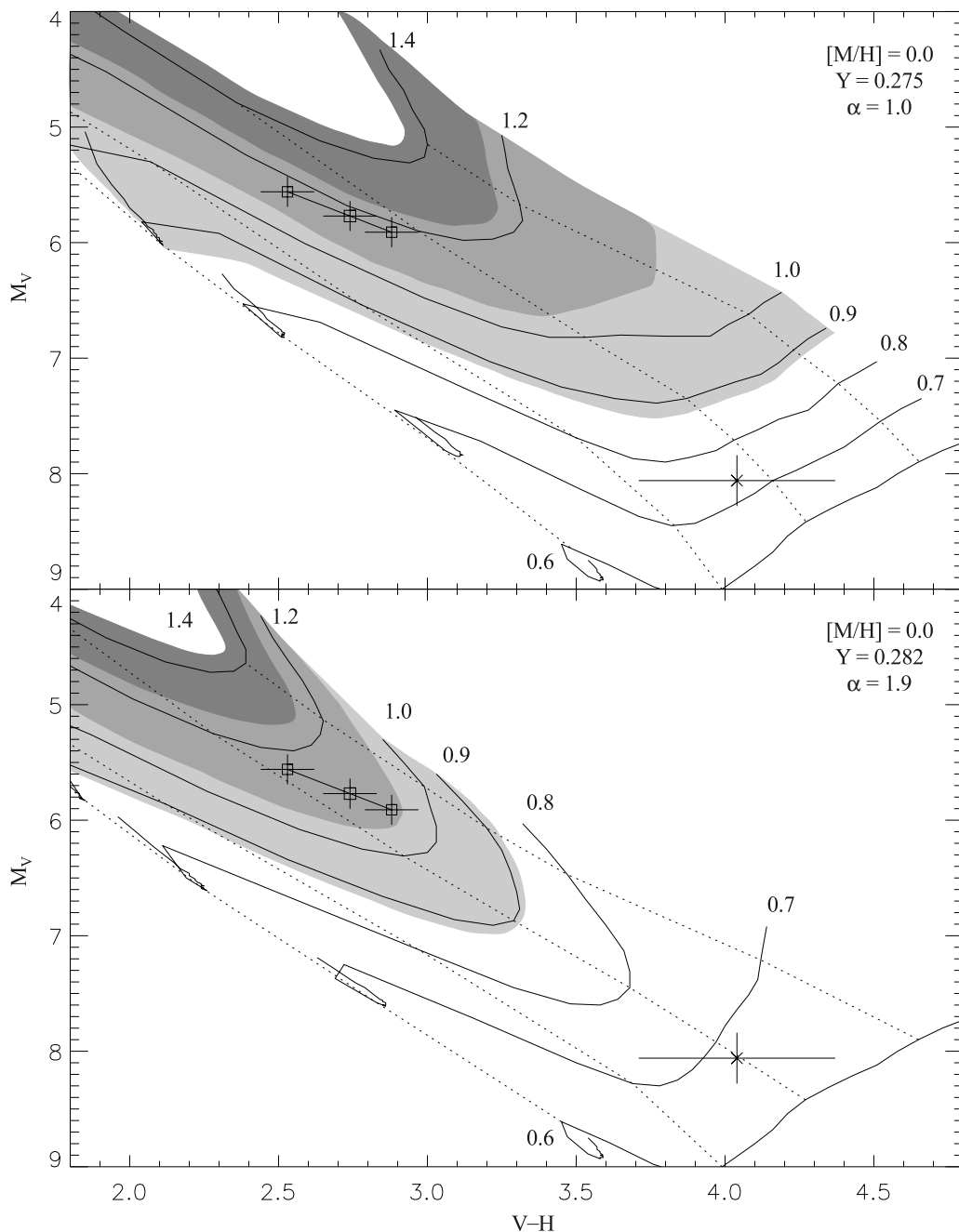


FIG. 4.—Comparison of Baraffe et al. (1998) PMS tracks with NTT 045251+3016. The metallicity, helium abundance, and mixing-length parameter of each set of tracks are shown. The central open square on each figure represents the intrinsic magnitude and color of NTT 045251+3016, corrected for extinction and distance as described in the text. The other two open squares represent the range in these corrections within a K5 spectral type. The horizontal error bars represent  $1\sigma$  photometric uncertainties, and the vertical error bars represent both the combination of the two photometric and distance uncertainties. The solid lines are pre-main-sequence evolutionary tracks for stellar masses as labeled. Regions with model masses within  $1.0$ ,  $2.0$ , and  $3.0\sigma$  from our dynamical primary mass measurement of  $1.45 \pm 0.19 M_{\odot}$  are shaded from dark to light, respectively. The dotted lines are isochrones starting at  $3.16 \times 10^6$  yr and increasing by a factor of  $10^{0.5}$  yr. The secondary is plotted with a cross, and its error bars represent  $1.0\sigma$  observational errors. (The  $1.2$  and  $1.4 M_{\odot}$  tracks were provided by I. Baraffe (1999, private communication).

ondary, which is within the  $2.0\sigma$  range about our measured dynamical mass of the secondary. The primary star is estimated to be around  $6 \times 10^6$  yr old, while the secondary is about  $10^7$  yr old. However, the stars are within  $1.0\sigma$  of being coeval. The larger observational error on the secondary, compared with the error on the primary, is the limiting factor in comparing the calibration of the isochrones.

Palla & Stahler's (1999) PMS tracks give the mass of the secondary to be  $0.35 M_{\odot}$ , to be compared with our mea-

sured value for the secondary mass of  $0.81 M_{\odot}$ . At this position among the PS99 tracks, the predicted mass of the secondary depends only on  $T_{\text{eff}}$ . A  $1.0\sigma$  variation on  $T_{\text{eff}}$  corresponds to a change in mass of  $0.15 M_{\odot}$ . Even when combined with the error on the dynamical mass of the secondary of  $0.09 M_{\odot}$ , the mass predicted by the PS99 tracks is  $2.5\sigma$  from our measured dynamical mass.

Interestingly, the isochrones provided by PS99 suggest the largest relative age difference in the two stars among the

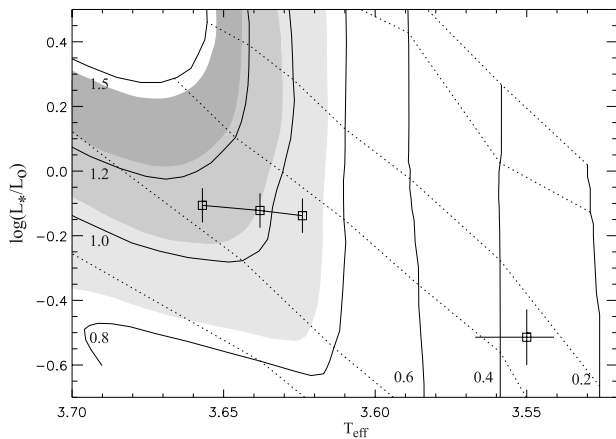


FIG. 5.—Palla & Stahler (1999) PMS tracks. Data are as in Fig. 4, except presented in  $\log(T_{\text{eff}})$ - $\log(L_*/L_\odot)$  domain. The dotted lines are isochrones that start at  $1 \times 10^5$  yr and increase in steps of  $10^{0.5}$  yr.

tracks tested in this paper. Using the PS99 isochrones, the primary is over  $6 \times 10^6$  yr old, while the secondary is only  $1.6 \times 10^6$  yr old. However, these age determinations are only distinct between the 1 and 2  $\sigma$  confidence level.

The DM97 tracks also give a mass for the secondary of  $0.34 M_\odot$ . As with the PS99 tracks, the secondary's location with respect to the DM97 tracks makes the predicted mass sensitive primarily to changes in  $T_{\text{eff}}$ . A  $1.0 \sigma$  change in  $T_{\text{eff}}$  corresponds to a change in predicted mass of  $0.1 M_\odot$ . Combining this uncertainty with the error on the measured mass, we find that the secondary mass predicted by the DM97 tracks is at least 3  $\sigma$  from the dynamical mass. The DM97 isochrones give the ages of both the primary and secondary stars to be  $1.8 \times 10^6$  yr and  $10^6$  yr, respectively. These ages are within 1  $\sigma$  of being coeval.

## 5. CONCLUSION

In this paper, we present dynamical masses for the components of the binary NTT 045251 + 3016. These mass measurements were derived from analysis of astrometric

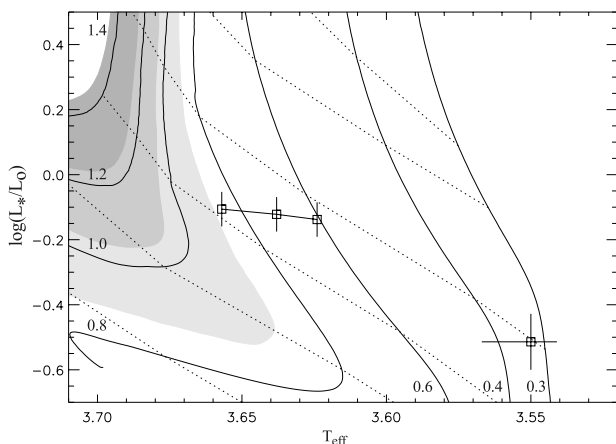


FIG. 6.—D'Antona & Mazzitelli (1997) PMS tracks. The data and curves are as in Fig. 5.

data from the *HST* FGS, optical spectroscopic data from the digital speedometers at CfA, and IR spectroscopic data from PHOENIX at KPNO. Our measured values for the primary and secondary masses are  $1.45 \pm 0.19$  and  $0.81 \pm 0.09 M_\odot$ , respectively, at a distance of  $145 \pm 8$  pc. The uncertainties in these mass measurements can be readily reduced by more numerous measurements of the secondary radial velocity, which we encourage.

The measured primary and secondary masses are compared with predicted masses of three sets of PMS tracks: Baraffe et al. (1998), Palla & Stahler (1999), and D'Antona & Mazzitelli (1997). The Baraffe et al. (1998) tracks that use the Next Gen nongray atmosphere models of Hauschildt et al. 1999 and a mixing-length parameter  $\alpha = 1.0$  provide the closest agreement with our results. The masses predicted by the models deviate between 1.3 and 1.6  $\sigma$  from our measured primary mass and less than 1.0  $\sigma$  from our measured secondary mass. The Baraffe et al. (1998) tracks with  $\alpha = 1.9$  predict a primary mass that is between 1.6 and 2.1  $\sigma$  from our measured primary mass and a secondary mass that is within 2  $\sigma$  of our dynamical value. The PMS tracks of Palla & Stahler (1999) give a primary mass range that deviates 1.6–2.9  $\sigma$  from our dynamical primary mass, and the predicted secondary mass is 2.5  $\sigma$  from our dynamical value. Finally, the values for the primary and secondary masses provided by the tracks of D'Antona & Mazzitelli (1997), who use the FST to model stellar convection rather than standard MLT, deviate by more than 3.0  $\sigma$  from our measured dynamical masses. We therefore conclude that the Baraffe et al. (1998) and Palla & Stahler (1999) models are consistent with our observations of NTT 045251 + 3016, while the D'Antona & Mazzitelli (1997) tracks are inconsistent at a significant confidence level.

If we assume the binary system is coeval, we can use our observations to constrain the relative accuracy of the isochrones provided by each PMS model. All three PMS models tested are consistent with coeval formation of both components. Better determination of the effective temperatures of the component stars will be needed to provide a tighter constraint on the PMS isochrones.

All the PMS evolutionary tracks tested in this paper underestimate the masses of both the primary and secondary stars. The secondary star lies amidst the Hayashi tracks, and our observations demand cooler effective temperatures for the  $0.8 M_\odot$  tracks. The same is true for the primary star when compared with the D'Antona & Mazzitelli models. However, when compared with the Baraffe et al. and Palla & Stahler tracks, the primary lies at the transition between the convective and radiative tracks. For these models, our observations of the primary star require both cooler temperatures and lower luminosities. This need for cooler effective temperatures from the evolutionary models is similar to the recent findings of Simon et al. (2000). Interestingly, D'Antona, Ventura, & Mazzitelli (2000) argue that the effective temperatures predicted by present PMS evolutionary models are actually upper limits, because magnetic fields, which are not included in any of the models tested here, act to reduce effective temperature.

We are indebted to the Space Telescope Science Institute, and especially the FGS team, for superb technical support throughout this program and for funding support. We also thank the many CfA observers who have obtained observations over the 15 years of this program and E. Goldberg

for helping with the TODCOR analysis. Finally, the generous contribution of software from G. Torres, analyses and expertise from C. Dolan, and additional evolutionary tracks from I. Baraffe were invaluable. The work of Tsevi Mazeh

was supported by US-Israel Binational Science Foundation grant 97-00460 and the Israel Science Foundation. The work of Lisa Prato and Michal Simon was supported, in part, by US NSF grant 98-19694.

## REFERENCES

- Alexander, D. R., & Ferguson, J. W. 1994, *ApJ*, 437, 879  
 Baraffe, I., Chabrier, G., Allard, F., & Hauschildt, P. H. 1998, *A&A*, 337, 403 (BCAH98)  
 Basri, G., & Batalha, C. 1990, *ApJ*, 363, 654  
 Batten, A. H. 1973, in *Binary and Multiple Systems of Stars* (Oxford: Pergamon Press)  
 Bernacca, P. L., Lattanzi, M. G., Bucciarelli, B., Barabaro, G., Pannunzio, R., Badiali, M., Cardini, D., & Emanuele, A. 1993, *A&A*, 278, L47  
 Bertout, C., Robichon, N., & Arenou, F. 1999, *A&A*, 352, 574  
 Canuto, V. M., Goldman, I., & Mazzitelli, I. 1996, *ApJ*, 473, 550  
 Canuto, V. M., & Mazzitelli, I. 1991, *ApJ*, 370, 295  
 Casey, B. W., Mathieu, R. D., Vaz, L. P. R., Andersen, J., & Suntzeff, N. B. 1998, *AJ*, 115, 1617  
 Corporon, P., Lagrange, A. M., & Beust, H. 1996, *A&A*, 310, 228  
 Covino, E., et al. 2000, *A&A*, 361, L49  
 D'Antona, F., & Mazzitelli, I. 1997, *Mem. Soc. Astron. Italiana*, 68, 807 (DM97)  
 D'Antona, F., Ventura, P., & Mazzitelli, I. 2000, *ApJ*, 543, L77  
 Guilleaume, S., Dutrey, A., & Simon, M. 1999, *A&A*, 348, 570  
 Hartigan, P., Strom, K. M., & Strom, S. E. 1994, *ApJ*, 427, 961  
 Hartmann, L., Hewett, R., Stahler, S., & Mathieu, R. D. 1986, *ApJ*, 309, 275  
 Hauschildt, P. H., Allard, F., Baron, E. 1999, *ApJ*, 512, 377  
 Iglesias, C. A., & Rogers, F. J. 1996, *ApJ*, 464, 943  
 Kenyon, S. J., Dobrzycka, D., & Hartmann, L. 1994, *AJ*, 108, 1872  
 Kenyon, S. J., & Hartmann, L. 1995, *ApJS*, 101, 117  
 Kurtz, M. J., & Mink, D. J. 1998, *PASP*, 110, 934  
 Latham, D. W. 1992, in *ASP Conf. Ser. 32, Complementary Approaches to Double and Multiple Star Research*, ed. H. McAlister & W. Hartkopf (IAU Colloq. 135) (San Francisco: ASP), 110  
 Lattanzi, M. G., Munari, U., Whitelock, P. A., & Feast, M. W. 1997, *ApJ*, 485, 328  
 Lee, C. W. 1992, Ph.D. thesis, Univ. Wisconsin, Madison  
 Lupie, O. L., & Nelan, E. P. 1998, *FGS Instrument Handbook*, Version 7 (Washington, D. C.: AURA, Inc.)  
 Mazeh, T., Prato, L., Simon, M., & Goldberg, E. 2000a, in *Birth and Evolution of Binary Stars: Poster Proc. of IAU Symp. 200*, ed. B. Reipurth & H. Zinnecker (San Francisco: ASP), 22  
 Mazeh, T., Prato, L., Simon, M., & Goldberg, E. 2001, in preparation  
 Morse, J. A., & Kurucz, R. L. 2001, in preparation  
 Palla, F., & Stahler, S. W. 1999, *ApJ*, 525, 772 (PS99)  
 Simon, M., Dutrey, A., & Guilleaume, S. 2000, *ApJ*, 545, 1034  
 Walter, F. W., Brown, A., Mathieu, R. D., Myers, P. C., & Vrba, F. J. 1988, *AJ*, 96, 297  
 Wichmann, R., Bastian, U., Krautter, I., Jankovics, I., & Rucinski, S. M. 1998, *MNRAS*, 301, L39  
 Zucker, S., & Mazeh, T. 1994, *ApJ*, 420, 806